LETTER

Rectification of self-propelled cells in confluent tissues

To cite this article: Bao-quan Ai *et al* 2021 *EPL* **136** 58002

A Letters Journal Exploring the Frontiers of Physics

December 2021

EPL, **136** (2021) 58002 www.epljournal.org
doi: 10.1209/0295-5075/ac2539

Rectification of self-propelled cells in confluent tissues

Bao-quan Ai[1,2(a)], Guo-hao Xu[1,2], Jia-jian Li[1,2] and Ya-feng He[3(b)]

[1] *Guangdong Provincial Key Laboratory of Quantum Engineering and Quantum Materials, School of Physics and Telecommunication Engineering, South China Normal University - Guangzhou 510006, China*
[2] *Guangdong-Hong Kong Joint Laboratory of Quantum Matter, South China Normal University Guangzhou 510006, China*
[3] *Hebei Key Laboratory of Optic-electronic Information Materials, College of Physics Science and Technology, Hebei University - Baoding 071002, China*

received 10 May 2021; accepted in final form 9 September 2021
published online 1 March 2022

Abstract – Collective cell transport in dense tissues governs many biological processes, such as embryonic development, cancer metastasis and wound healing. How to control the directed transport of cells in dense tissues is still an interesting and open question. We numerically investigated the directed transport of a confluent tissue containing self-propelled cells in an asymmetric periodic potential by using the self-propelled Voronoi model. We demonstrate that cells in the confluent tissue can be rectified and the movement direction of cells is determined by the asymmetry of the potential. The cell shape index determines the state of the system and plays a central role in the rectification. There exists an optimal shape index at which the average velocity takes its maximal value. Interestingly, there exist two optimal self-propulsion speeds at which the average velocity reaches its maximum, which is different from the single-cell case (only one optimal speed). In addition, the average velocity is a peaked function of the cell number for small shape index and monotonously decreases with the increase of the cell number for large shape index. Our findings are relevant to the experimental pursuit of the control of motile confluent tissues on periodic substrates.

Introduction. – Biological processes including embryonic development, cancer metastasis and wound healing require cells to move collectively in dense tissues [1,2], which is very different from isolated cell motion. Several models have been proposed to describe the dynamics of cells in tissues [3–13] such as particle-based models [3,4], cellular Potts models [5], phase field models [6,7], and vertex models [8–13]. Vertex models are a class of such models that consider cells as individual objects, approximated by two-dimensional polygons representing cellular interfaces, which are highly successful in describing the motion of two-dimensional confluent cell tissues. A recent theoretical work [14] has combined the vertex model with ideas from active matter physics to develop a self-propelled Voronoi model of a motile tissue. Based on vertex or Voronoi models, researchers have successfully studied the dynamic properties of cells in dense tissues, such as jamming and glass transitions [14–27], mechanical heterogeneity [28–30], and collective transport [31–35].

Although many studies have involved collective transport of the tissue [31–35], how to manipulate the overall movement of the motile tissue is still an open and interesting question. The ratchet model provides a strategy to control the movement of particles driven by nonequilibrium fluctuations [36–44]. The ratchet setup can convert the random motion into the directional motion of particles, *i.e.*, so-called rectification. In the strongly collective limit, ratchet reversals were found in systems with asymmetric substrates [45,46]. Especially, in active matter ratchet systems [47–50], the interactions between particles are important and induce current reversals. Most previous work on rectification was based on particulate matter. However, the dense tissues are different from particulate matter in that the interactions between cells are shape based, as opposed to metric based. Therefore, it would be interesting to study the rectification of cells in the dense tissue, where there are no gaps between cells and the packing fraction is precisely at unity. In this paper, we study the directed transport of a confluent tissue containing self-propelled cells in an asymmetric periodic potential by using the self-propelled Voronoi model. It is found that

(a) E-mail: aibq@scnu.edu.cn (corresponding author)
(b) E-mail: heyf@hbu.edu.cn

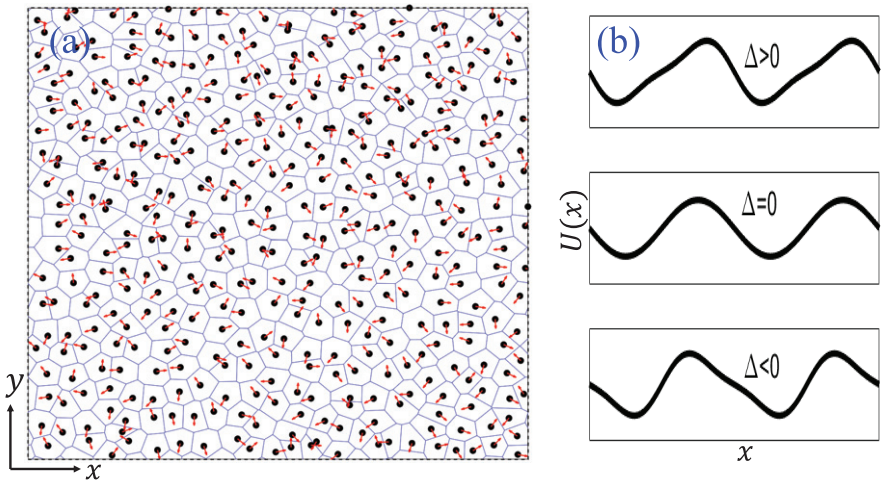

Fig. 1: (a) Schematic of a confluent tissue containing N self-propelled cells in a square box of side L with periodic boundary conditions. The red arrows describe the self-propulsion direction. (b) The profile of the potential $U(x)$ described in eq. (4) for different Δ. The left-hand side of the potential is steep when $\Delta > 0$ and the right-hand side is steep when $\Delta < 0$.

the motile confluent tissue could be manipulated by introducing an asymmetric periodic potential. The shape index plays a key role in rectification and there exists an optimal shape index at which the average velocity takes its maximal value. There exist two optimal self-propulsion speeds at which the average velocity reaches its maximal value. The average velocity is a peaked function of the cell number for small shape index and monotonously decreases with the increase of the cell number for large shape index.

Model and Methods. – We consider a confluent tissue containing N self-propelled cells (no cell divisions or apoptosis) in a square box of side L with periodic boundary conditions (shown in fig. 1(a)). Because the Voronoi-based cellular model is highly successful in describing the motion of two-dimensional confluent cell tissues [14,15], we use the self-propelled Voronoi model to study the dynamics of motile confluent tissues. In the Voronoi model, the basic degrees of freedom are the set of two-dimensional cell centers $\{\mathbf{r}_i = (x_i, y_i)\}$, and cell shapes are given by the resulting Voronoi tessellation. The tissue forces are obtained from an effective energy functional $E(\{\mathbf{r}_i\})$ for N cells, given by [8–21]

$$E = \sum_{i=1}^{N} E_i, E_i = K_A[A_i - A_0]^2 + K_p[P_i - P_0]^2, \qquad (1)$$

where A_i and P_i are the cross-sectional area and perimeter of the cell i. A_0 and P_0 are the preferred cell area and perimeter values at which the energy is minimized. We assume that the preferred cell area A_0 does not vary from cell to cell and is set to be the average area per cell. K_A and K_P represent the area and perimeter stiffness moduli, respectively. The first term results from a combination of cell volume incompressibility and the monolayer's resistance to height fluctuations [51]. The second term arises from active contractility of the actomyosin subcellular cortex and effective cell membrane tension due to cell-cell adhesion and cortical tension. An important parameter in the model is the dimensionless shape index $p_0 = P_0/\sqrt{A_0}$. For example, a regular hexagon has a dimensionless shape index of $p_0 \approx 3.72$.

In the self-propelled Voronoi model, each cell can move due to self-propelled motility. A constant self-propulsion speed v_0 is assigned along the direction of polarization $\hat{\mathbf{n}} = (\cos\theta_i, \sin\theta_i)$ to each cell. In addition, in order to achieve the rectification of cells, each cell experiences a substrate force $\mathbf{G}_i^x$ along the x-direction which arises from a periodic potential $U(x)$. With these forces, the dynamics of each Voronoi cell center $\mathbf{r}_i$ are governed by the following overdamped Langevin equations:

$$\frac{\mathrm{d}\mathbf{r}_i}{\mathrm{d}t} = \mu[\mathbf{F}_i + \mathbf{G}_i^x] + v_0\hat{\mathbf{n}}, \qquad (2)$$

$$\frac{\mathrm{d}\theta_i}{\mathrm{d}t} = \sqrt{2D_r}\xi_i(t), \qquad (3)$$

where μ is the mobility. $\mathbf{F}_i = -\nabla_i E$ is the effective mechanical interaction force on cell i, which is nonlocal and nonadditive. Different from the particle-based models, $\mathbf{F}_i$ cannot be expressed as the sum of pairwise force between cell i and its neighboring cells. $\xi_i(t)$ is the Gaussian white noise with zero mean and unit variance. D_r is the rotational diffusion constant and the time scale $\tau = 1/D_r$ controls the persistence of single-cell dynamics. The translational diffusion is assumed to be negligibly small, thus we do not consider the translational diffusion in the model.

The profile of the potential $U(x)$ (shown in fig. 1(b)) is described by

$$U(x) = -U_0\left[\sin\left(\frac{2\pi x}{L}\right) + \frac{\Delta}{4}\sin\left(\frac{4\pi x}{L}\right)\right], \qquad (4)$$

where U_0 and L are the height and period of the potential, respectively. Δ is the asymmetric parameter of the

potential in the x-direction and the potential is completely symmetric at $\Delta = 0$.

Equations (1)–(4) can be rewritten in the dimensionless forms by introducing the characteristic length $\sqrt{A_0}$ and time $1/(\mu K_A A_0)$. The parameters in the dimensionless forms can be rewritten as $\hat{v}_0 = v_0/(\mu K_A A_0^{3/2})$, $\hat{D}_r = D_r/(\mu K_A A_0)$, $\hat{U}_0 = U_0/(K_A A_0^2)$, $\hat{K}_P = K_P/(K_A A_0)$, $\hat{L} = L/\sqrt{A_0}$. From now on, we will use only the dimensionless variables and shall omit the hat for all quantities occurring in the above equations.

Because directed transport only occurs in the x-direction, the average velocity of the particle along the x-direction in the asymptotic long-time regime can be obtained from the following formula:

$$V_x = \lim_{t\to\infty} \frac{1}{N} \sum_{i=1}^{N} \frac{\langle x_i(t)\rangle}{t}, \tag{5}$$

where the symbol $\langle \ldots \rangle$ denotes an average over the random initial conditions.

Results and discussion. – We solve numerically eqs. (2), (3) by using a stochastic Runge-Kutta algorithm. The time step is chosen to be smaller than 0.01 and the total integration time is more than 5×10^6. The stochastic averages are obtained as ensemble averages over 100 trajectories with random initial conditions. For convenience, we set the average cell area $\bar{A} = L^2/N$ equal to one, thus $L = \sqrt{N}$. Unless otherwise noted, we set $K_P = 1$, $N = 400$, and $U_0 = L/2\pi$ throughout the simulations. In the following, we explore the ratchet transport of cells by varying the asymmetry parameter Δ, the shape index p_0, the self-propulsion speed v_0, and the rotational diffusion constant D_r.

First, we plot the solid-liquid phase diagram as a function of v_0 and p_0 for different cases in fig. 2. Cell shape is a structural order parameter for the solid-liquid transition. We define the structural order parameter based on cell shapes $q = \frac{1}{N}\sum \frac{P_i}{\sqrt{A_i}}$, which was shown to be an excellent order parameter for the solid-liquid transition in the self-propelled Voronoi model [14]. The solid-liquid transition is identified by the structural order parameter $q = 3.81$. It is found that the appearance of the external potential makes it easier for the system to behave as a liquid. This is because cells are isotropic in solid state and anisotropic in liquid state and the external potential will cause the system to become anisotropic. In order to obtain the rectification of cells, the system should be in liquid state. Therefore, most of the parameters we use can ensure that the system is in liquid state.

Figure 3(a) shows the average velocity V_x of cells as a function of the asymmetry parameter Δ for different p_0. We find that the average velocity V_x is positive when $\Delta > 0$, zero at $\Delta = 0$ and negative when $\Delta < 0$. When the potential is completely symmetric (shown in the middle panel of fig. 1(b)), the probabilities of crossing the right and left barriers are the same, so that the average

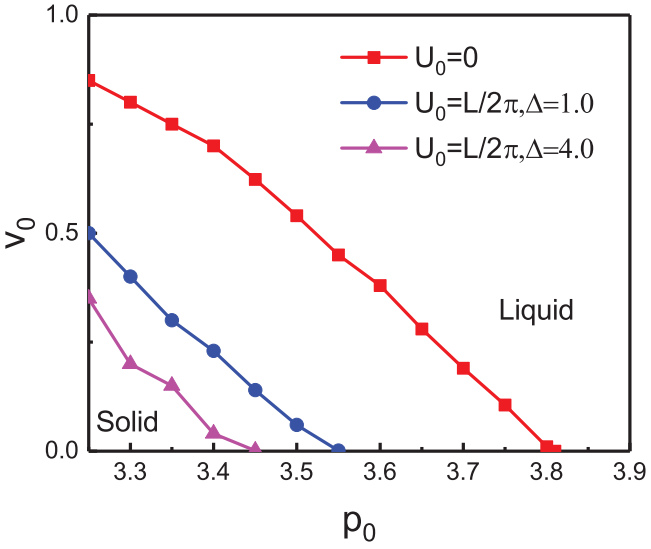

Fig. 2: The solid-liquid transition in the v_0-p_0 phase space for different cases at $D_r = 0.001$. Lines represent the solid-liquid transition identified by the structural order parameter $q = 3.81$.

velocity V_x is equal to zero. When $\Delta > 0$, the left side from the minima of the potential is steeper (shown in the top panel of fig. 1(b)), and it is easier for cells to move toward the slanted side than toward the steep side, so cells on average move to the right ($V_x > 0$). Similarly, cells on average move to the left ($V_x < 0$) when $\Delta < 0$. Therefore, the asymmetric orientation of the potential determines the movement direction of cells. In addition, when $|\Delta|$ is very large, the effective height of the potential is too high for cells to pass across the potential barrier, so V_x tends to zero. Therefore, there exists an optimal value of $|\Delta|$ at which V_x takes its maximal value. In the discussion below, we only consider the case of $\Delta > 0$.

Figure 3(b) describes the average velocity V_x as a function of the self-propulsion speed v_0 for different p_0 at $\Delta = 4.0$. In order to investigate the role of the interactions between cells, we calculate the average velocity for a single-cell case (denoted by the solid line in fig. 3(b)), where $K_A = 0$ and $K_P = 0$. For the single-cell case, the average velocity is always zero when $v_0 < 2.0$ (particles cannot pass across the potential barrier) and there is a peak in the curve when $v_0 > 2.0$. However, when the shape-based interactions are considered, there are two peaks in each curve, which are, respectively, distributed in the region $v_0 < 2.0$ and the region $v_0 > 2.0$. The first peak is due to the shape-based interactions.

A qualitative explanation of the behaviors in fig. 3(b) is presented as follows. When $v_0 < 2.0$, the effective mechanical interaction force (determined by the shape index p_0) plays an important role in the dynamics of cells. The competition between the self-propulsion speed v_0 and the shape index p_0 determines the rectification of cells. In this case, when $v_0 \to 0$, cells cannot pass across the potential

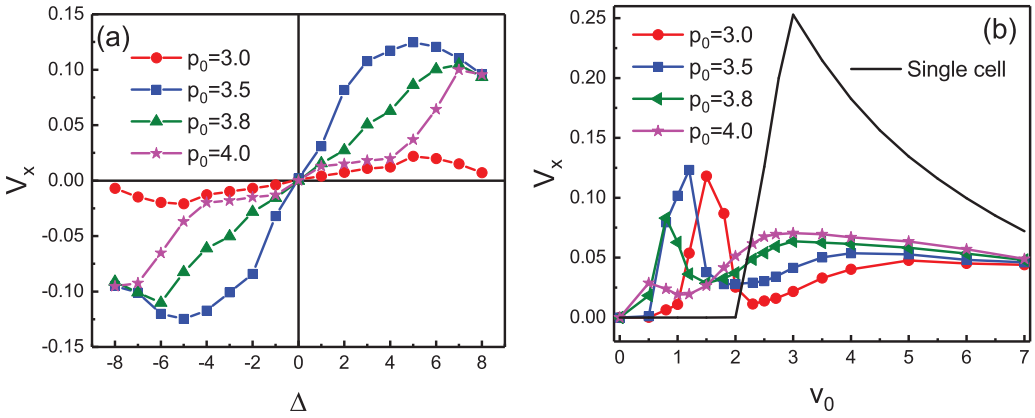

Fig. 3: (a) Average velocity V_x as a function of the asymmetry parameter Δ for different shape index p_0 at $v_0 = 1.0$ and $D_r = 0.001$. (b) Average velocity V_x as a function of the self-propulsion speed v_0 for different p_0 at $\Delta = 4.0$ and $D_r = 0.001$. The solid line denotes the single cell case, where $K_A = 0$ and $K_P = 0$.

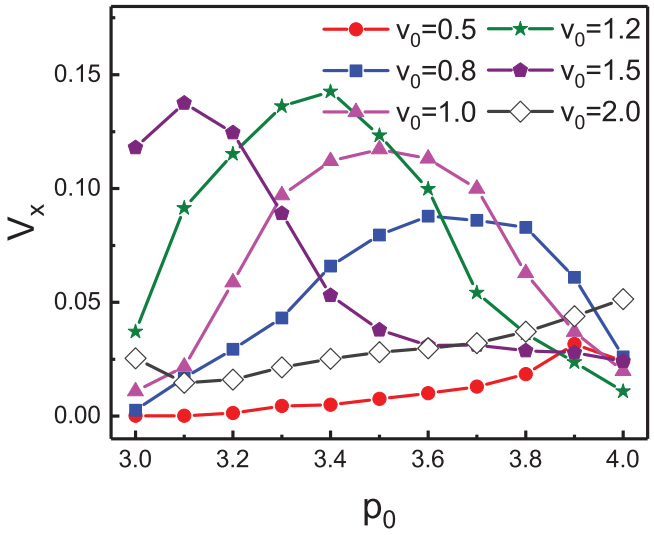

Fig. 4: Average velocity V_x as a function of the shape index p_0 for different v_0 at $\Delta = 4.0$ and $D_r = 0.001$.

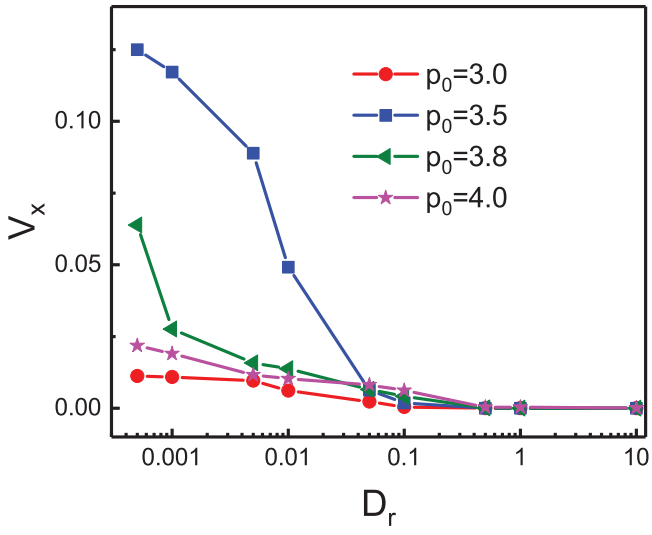

Fig. 5: Average velocity V_x as a function of the rotational diffusion constant D_r for different shape index p_0 at $v_0 = 1.0$ and $\Delta = 4.0$.

barrier, thus $V_x \to 0$. As v_0 increases, cells begin to pass across the potential barrier and rectification occurs. However, when v_0 increases to larger values, cells can easily pass across the potential barrier, which reduces the effect of the asymmetry potential, so V_x decreases. Therefore, in this case, there exists an optimal value of v_0 at which V_x is maximal. In addition, the position of the peak shifts to small v_0 as p_0 is increased. When $v_0 > 2.0$, the self-propelled motility is large enough and each cell can move freely and the self-propelled motility dominates the dynamics of cells. In this case, on increasing v_0, the average velocity V_x firstly increases to its maximum, and then decreases to zero, thus there is a peak in each curve. Similar to the previous case, the position of the peak also shifts to small v_0 as p_0 is increased. Note that when v_0 reaches to a certain value (*e.g.*, $v_0 = 7.0$), the effect of the shape index can be negligible, all curves p_0 will completely coincide.

The dependence of the average velocity V_x on the shape index p_0 is shown in fig. 4 for different v_0 at $\Delta = 4.0$. It is found that the average velocity V_x is a peaked function of the shape index p_0. Note that the peak in the curve for $v_0 = 2.0$ will appear in the range of $p_0 < 3.0$, which is not shown in fig. 3. The emergence of the peak in each curve can be explained as follows. The system exhibits a jamming transition from a solid-like state to a fluid-like state [14], which is determined by the shape index, the self-propelled motility, and the rotational diffusion constant. When p_0 is small, the system shows the solid-like state and it is very difficult for cells to pass across the potential barrier, thus V_x is very small. When p_0 is large, the system shows the fluid-like state, the self-propelled motility dominates the transport. Cells can pass across the potential barrier easily and the effect of the potential can be negligible, so the rectification of cells is very weak.

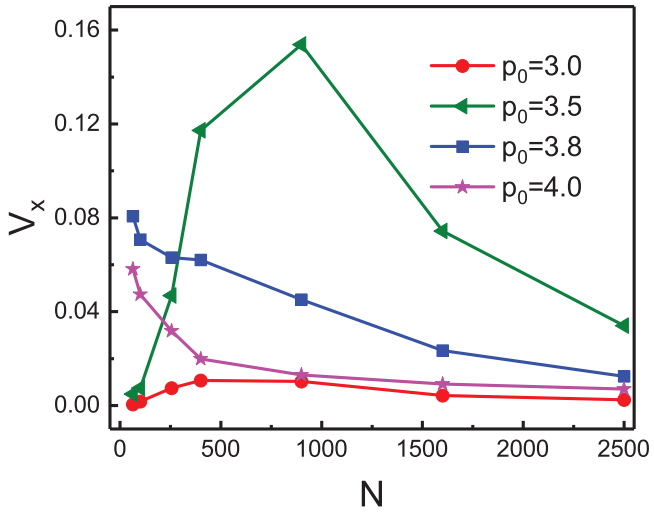

Fig. 6: Average velocity V_x as a function of the cell number N for different p_0 at $v_0 = 1.0$, $\Delta = 4.0$, and $D_r = 0.001$.

Therefore, there exists an optimal value of p_0 at which V_x takes its maximal value, which is different from the single-cell case. In addition, the position of the peak shifts to small p_0 with an increase in v_0. This is because the shape index p_0 at the solid-liquid transition decreases with the increase of v_0. Therefore, the shape index determines the state of the system and strongly affects the rectification of cells.

Figure 5 depicts the average velocity V_x as a function of the rotational diffusion constant D_r for different p_0 at $v_0 = 1.0$ and $\Delta = 4.0$. In the adiabatic limits $D_r \to 0$, the self-propelled velocity can be expressed by two opposite static velocity v_0 and $-v_0$, which is similar to the adiabatic case in the force thermal ratchet [36], thus V_x is large. As D_r increases, the average velocity V_x decreases. When $D_r \to \infty$, the time scale $\tau = 1/D_r \to 0$, eq. (2) approaches simple Brownian motion and the nonequilibrium driving disappears, thus V_x tends to zero. Therefore, on increasing D_r from zero, the average velocity V_x monotonically decreases and finally tends to zero.

In fig. 6, we show how the cell number N affects the average velocity V_x for different p_0 at $v_0 = 1.0$ and $\Delta = 4.0$. It is found that the average velocity V_x is a peaked function of N for small p_0 and monotonously decreases with the increase of N for large p_0. This can be explained as follows. An increase of the cell number N can cause two results: a) activating motion in analogy with the thermal noise activated motion for a single stochastically driven ratchet, which facilitates the rectification of cells and b) reducing the effective mobility of cells, which blocks the rectification of cells. When p_0 is small (*e.g.*, $p_0 = 3.0$ and 3.5), the effective mobility of each cell is small and cells cannot easily pass the potential barrier. In this case, on increasing N from zero, the factor a) first dominates the transport, so V_x increases with N. However, when N is very large and the effective mobility of each cell is reduced, which blocks the rectification of cells, thus V_x decreases with the increase of N. Therefore, there exists an optimal cell number at which the average velocity V_x is maximal. When p_0 is large (*e.g.*, $p_0 = 3.8$, and 4.0), the system shows the fluid-like state and cells can easily pass the potential barrier. In this case, the factor b) always dominates the transport, V_x monotonously decreases with the increase of N.

Concluding remarks. – In this paper, we numerically study the directed transport of a confluent tissue containing self-propelled cells in an asymmetry periodic potential by using the self-propelled Voronoi model. We can manipulate the movement of cells in the dense tissue by introducing the asymmetric periodic potential. The movement direction of cells is determined by the asymmetry of the potential, the average velocity is positive for $\Delta < 0$, zero at $\Delta = 0$ and negative for $\Delta > 0$. Because the shape index determines the state of the active tissue, it strongly affects the rectification of cells. The average velocity is a peaked function of the shape index and the position of the peak shifts to small shape index when the self-propulsion speed is increased. The self-propelled motility of each cell is another important factor in determining the state of the system. When $v_0 < 2.0$, the competition between the self-propulsion and the shape index determines the rectification of cells, so there is an optimal value of v_0 at which V_x takes its extreme value. When $v_0 > 2.0$, the self-propelled motility dominates the rectification, there is another optimal value of v_0 at which V_x is extreme. Therefore, there exist two optimal self-propulsion speeds in different speed ranges. The rotational diffusion constant D_r controls the persistence of single-cell dynamics and the the persistent time decreases with increasing D_r. Therefore, the average velocity monotonically decreases with the increase of D_r and tends to zero when $D_r \to \infty$. In addition, the cell number can also affect the rectification of cells, the average velocity is a peaked function of the cell number for small shape index and monotonously decreases with the increase of the cell number for large shape index.

Our study suggests the possibility to manipulate motile confluent tissues on periodic substrates, which provides a theoretical framework for predicting manipulation of cells in cancer tumorogenesis, embryogenesis, and wound healing. In addition, most previous work on rectification was based on particulate matter, here we have achieved rectification of cells in dense tissues, where the interactions between the cells are shape based and the packing fraction is precisely at unity. We hope that our results can be realized in the experiments of motile confluent tissues on periodic substrates.

* * *

This work was supported in part by the National Natural Science Foundation of China (Grants Nos.

12075090 and 11975089), Science and Technology Program of Guangzhou (Grant No. 2019050001), the Natural Science Foundation of Guangdong Province (Grant No. 2017A030313029), and the Major Basic Research Project of Guangdong Province (Grant No. 2017KZDXM024).

Data availability statement: The data generated and/or analysed during the current study are not publicly available for legal/ethical reasons but are available from the corresponding author on reasonable request.

REFERENCES

[1] Angelini T. E., Hannezo E., Trepat X., Marquez M., Fredberg J. J. and Weitz D. A., *Proc. Natl. Acad. Sci. U.S.A.*, **108** (2011) 4714.
[2] Angelini T. E., Hannezo E., Trepat X., Fredberg J. J. and Weitz D. A., *Phys. Rev. Lett.*, **104** (2010) 168104.
[3] Smeets B., Alert R., Pesek J., Pagonabarraga I., Ramon H. and Vincent R., *Proc. Natl. Acad. Sci. U.S.A.*, **113** (2016) 14621.
[4] Berthier L., *Phys. Rev. Lett.*, **112** (2014) 220602.
[5] Segerer F. J., Thüroff F., Piera Alberola A., Frey E. and J. O. Rädler, *Phys. Rev. Lett.*, **114** (2015) 228102.
[6] Camley B. A. and Rappel W. J., *J. Phys. D*, **50** (2017) 113002.
[7] Mueller R., Yeomans J. M. and Doostmohammadi A., *Phys. Rev. Lett.*, **122** (2019) 048004.
[8] Nagai T. and Honda H., *Phys. Rev. E*, **80** (2009) 061903.
[9] Kursawe J., Baker R. E. and Fletcher A. G., *J. Comput. Phys.*, **345** (2017) 752.
[10] Fletcher A. G., Osterfield M., Baker R. E. and Shvartsman S. Y., *Biophys. J.*, **106** (2014) 2291.
[11] Alt S., Ganguly P. and Salbreux G., *Philos. Trans. R. Soc. B*, **372** (2017) 20150520.
[12] Hakim V. and Silberzan P., *Rep. Prog. Phys.*, **80** (2017) 076601.
[13] Barton D., Henkes S., Weijer C. and Sknepnek R., *PLoS Comput. Biol.*, **13** (2017) e1005569.
[14] Bi D., Yang X., Marchetti M. C. and Manning M. L., *Phys. Rev. X*, **6** (2016) 021011.
[15] Bi D., Lopez J. H., Schwarz J. M. and Manning M. L., *Nat. Phys.*, **11** (2015) 1074.
[16] Li X., Das A. and Bi D., *Proc. Natl. Acad. Sci. U.S.A.*, **115** (2018) 6650.
[17] Yan L. and Bi D., *Phys. Rev. X*, **9** (2019) 011029.
[18] Giavazzi F., Paoluzzi M., Macchi M., Bi D., Scita G., Manning M. L., Cerbino R. and Marchetti M. C., *Soft Matter*, **14** (2018) 3471.
[19] Sussman D. M., Paoluzzi M., Marchetti M. C. and Manning M. L., *EPL*, **121** (2018) 36001.
[20] Sussman D. M. and Merkel M., *Soft Matter*, **14** (2018) 3397.
[21] Sussman D. M., *Comput. Phys. Commun.*, **219** (2017) 400.
[22] Sussman D. M., *Phys. Rev. Res.*, **2** (2020) 023417.
[23] Czajkowski M., Sussman D. M., Marchetti M. C. and Manning M. L., *Soft Matter*, **15** (2019) 9133.
[24] Atia L., Bi D., Sharma Y., Mitchel J. A., Gweon B., Koehler S. A., DeCamp S. J., Lan B., Kim J. H., Hirsch R., Pegoraro A. F., Lee K. H., Starr J. R., Weitz D. A., Martin A. C., Park J., Butler J. P. and Fredberg J. J., *Nat. Phys.*, **14** (2018) 613.
[25] Michael Moshe, Mark J. Bowick and Cristina Marchetti M., *Phys. Rev. Lett.*, **120** (2018) 268105.
[26] Boromand A., Signoriello A., Ye F., ÓHern C. S. and Shattuck M. D., *Phys. Rev. Lett.*, **121** (2018) 248003.
[27] Teomy E., Kessler D. A. and Levine H., *Phys. Rev. E*, **98** (2018) 042418.
[28] Sussman D. M., Schwarz J. M., Marchetti M. C. and Manning M. L., *Phys. Rev. Lett.* **120** (2018) 058001.
[29] Yang X., Bi D., Czajkowskic M., Merkel M., Lisa Manning M. and Marchetti M. C., *Proc. Natl. Acad. Sci. U.S.A.*, **114** (2017) 12663.
[30] Li X., Das A. and Bi D., *Phys. Rev. Lett.*, **123** (2019) 058101.
[31] Sunyer R., Conte V., Escribano J., Elosegui-Artola A., Labernadie A., Valon L., Navajas D., Garcia-Aznar J. M., Munoz J. J., Roca-Cusachs P. and Trepat X., *Science*, **353** (2016) 1157.
[32] Petrolli V., Goff M. L., Tadrous M., Martens K., Allier C., Mandula O., L. Hervé, Henkes S., Sknepnek R., Boudou T., Cappello G. and Balland M., *Phys. Rev. Lett.*, **122** (2019) 168101.
[33] Emma Lång, Polec A., Lång A., Valk M., Blicher P., Rowe A. D., Tønseth K. A., Jackson C. J., Utheim T. P., Janssen L. M. C., Eriksson J. and Bøe S. O., *Nat. Commun.*, **9** (2018) 3665.
[34] Koride S., Loza A. J. and Sun S. X., *APL Bioeng.*, **2** (2018) 031906.
[35] Trepat X. and Sahai E., *Nat. Phys.*, **14** (2018) 671.
[36] Hänggi P. and Marchesoni F., *Rev. Mod. Phys.*, **81** (2009) 387.
[37] Reimann P., *Phys. Rep.*, **361** (2002) 57.
[38] Olson Reichhardt C. J. and Reichhardt C., *Annu. Rev. Condens. Matter Phys.*, **8** (2017) 51.
[39] Ghosh P. K., Misko V. R., Marchesoni F. and Nori F., *Phys. Rev. Lett.*, **110** (2013) 268301.
[40] Li Y., Ghosh P. K., Marchesoni F. and Li B., *Phys. Rev. E*, **90** (2014) 062301.
[41] Ghosh P. K., Hänggi P., Marchesoni F. and Nori F., *Phys. Rev. E*, **89** (2014) 062115.
[42] He Y. F., Ai B. Q., Dai C. X., Song C., Wang R. Q., Sun W. T., Liu F. C. and Feng Y., *Phys. Rev. Lett.*, **124** (2020) 075001.
[43] Ai B. Q., Chen Q. Y., He Y. F., Li F. G. and Zhong W. R., *Phys. Rev. E*, **88** (2013) 062129.
[44] Ma X., Olson Reichhardt C. J. and Reichhardt C., *Phys. Rev. B*, **95** (2017) 104401.
[45] Mukhopadhyay A. K., Liebchen B. and Schmelcher P., *Phys. Rev. Lett.*, **120** (2018) 218002.
[46] Lu Q., Reichhardt C. J. O. and Reichhardt C., *Phys. Rev. B*, **75** (2007) 054502.
[47] McDermott D., Reichhardt C. J. O. and Reichhardt C., *Soft Matter*, **12** (2016) 8606.

[48] Wan M. B., Reichhardt C. J. O., Nussinov Z. and Reichhardt C., *Phys. Rev. Lett.*, **101** (2008) 018102.

[49] Bechinger C., Di Leonardo, R., Löwen, H., Reichhardt C., Volpe G. and Volpe G., *Rev. Mod. Phys.*, **88** (2016) 045006.

[50] Lau B., Kedem O., Schwabacher J., Kwasnieski D. and Weiss E. A., *Mater. Horiz.*, **4** (2017) 310.

[51] Hufnagel L., Teleman A. A., Rouault H., Cohen S. M. and Shraiman B. I., *Proc. Natl. Acad. Sci. U.S.A.*, **104** (2007) 3835.